Bone 89 (2016) 32–39

Contents lists available at ScienceDirect

Bone

journal homepage: www.elsevier.com/locate/bone

Full Length Article

Doses effects of zoledronic acid on mineral apatite and collagen quality of newly-formed bone in the rat's calvaria defect

Cécile Olejnik [a,b,c,*], Guillaume Falgayrac [a,b], Alexandrine During [a,b], Bernard Cortet [a,d], Guillaume Penel [a,b,c]

[a] Université de Lille, EA 4490 PMOI, F-59000 Lille, France
[b] Faculté de Chirurgie Dentaire, Place de Verdun, F-59000 Lille, France
[c] Service d'Odontologie, Centre Abel Caumartin, CHRU de Lille, F-59000 Lille, France
[d] Service de Rhumatologie, Hôpital Roger Salengro, CHRU de Lille, F-59000 Lille, France

ARTICLE INFO

Article history:
Received 1 December 2015
Revised 18 April 2016
Accepted 5 May 2016
Available online 7 May 2016

Keywords:
Bisphosphonate
Bone quality
Collagen
Mineral
Raman microspectroscopy
Rat

ABSTRACT

Due to their inhibitory effects on resorption, bisphosphonates are widely used in the treatment of diseases associated to an extensive bone loss. Yet, little is known about bisphosphonates effects on newly-formed bone quality. In the present study, adult male Sprague-Dawley rats ($n = 80$) with a bone defect *calvaria* area were used and short-term effects of zoledronic acid (ZA) were studied on the healing bone area. Three ZA treatments were tested by using either: 1°) a low single dose (120 μg ZA/kg, $n = 10$; equivalent to human osteoporosis treatment), 2°) a low fractionated doses (20 μg ZA/kg daily for 6 days either a total of 120 μg/kg, $n = 15$), and 3°) a high fractionated doses, (100 μg ZA/kg weekly for 6 weeks, $n = 15$; equivalent to 6 months of human bone metastasis treatment). For each treatment, a control "vehicle" treatment was performed (with an identical number of rats). After ZA administration, the intrinsic bone material properties were evaluated by quantitative backscattered electron imaging (qBEI) and Raman microspectroscopy. Neither single nor fractionated low ZA doses modify the intrinsic bone material properties of the newly-formed bone compared to their respective control animals. On the opposite, the high ZA treatment resulted in a significant decrease of the crystallinity (−25%, $P < 0.05$) and of the hydroxyproline-to-proline ratio (−30%, $P < 0.05$) in newly-formed bones. Moreover, with the high ZA treatment, the crystallinity was positively correlated with the hydroxyproline-to-proline ratio ($\rho = 0.78$, $P < 0.0001$). The present data highlight new properties for ZA on bone formation in a craniofacial defect model. As such, ZA at high doses disrupted the apatite crystal organization. In addition, we report here for the first time that high ZA doses decreased the hydroxyproline-to-proline ratio suggesting that ZA may affect the early collagen organization during the bone healing.

© 2016 Elsevier Inc. All rights reserved.

1. Introduction

Bisphosphonates (BPs) are known for their antiresorptive effects and their clinical properties related to the improvement of bone strength. BPs also show strong affinity for bone mineral, and their benefits are thought to be through their selective accumulation and improvement in bone quality, particularly in intrinsic bone material properties [1]. These effects were shown in bones going under remodeling with the increased organic and mineral bone tissue maturities. Yet, the remodeling suppression of BPs is only partial and some new bone matrix can be formed under treatment [2]. The newly-formed bone can be targeted by BPs because of the availability of the newly-formed mineral crystals for binding during BPs uptake and/or BPs recycling [3]. In addition, the potential adverse effects or interferences of BPs treatments on bone formation have been previously questioned in bone modeling [4–6], long bones fracture healing repair [7–9], *maxillae* bone healing [10–13] and osseointegration processes [14–16]. How BPs could affect the bone material properties in newly-formed bones remains unclear.

Zoledronic acid (ZA), a potent third-generation amino-BP, is currently known to have a higher mineral binding affinity and a higher antiresorptive activity than other BPs [17]. On actively forming bone surfaces, ZA has been previously shown to reverse deleterious post-menopausal osteoporotic effects as well as to exert also positive effects on bone quality on the younger bones [18,19]. This enhancement of the bone quality by ZA was suggested to be independent from its antiresorptive effects, possibly by improving directly bone formation and maturation. Nevertheless, the influence of ZA on bone matrix formation and mineralization needs to be explored.

The rodent *calvarial* bone defect is widely used to evaluate bone healing processes [20–22] or effects of various local factors on bone

Abbreviations: BE, back-scattered electrons; BMDD, bone mineralization density distribution; BP, bisphosphonate; CTL, control; GAG, glycosaminoglycan; PMMA, polymethyl methacrylate; qBEI, quantitative backscattered electron imaging; ROI, region of interest; ZA, zoledronic acid.

* Corresponding author at: EA 4490 PMOI, Faculté de Chirurgie Dentaire, Place de Verdun, F-59000 Lille, France.
E-mail address: cecile.olejnik-2@univ-lille2.fr (C. Olejnik).

http://dx.doi.org/10.1016/j.bone.2016.05.002
8756-3282/© 2016 Elsevier Inc. All rights reserved.

formation [23–25]. This craniofacial bone site in rodent represents a suitable alternative model to evaluate bone formation without mechanical loading of the bone due to its localization [26]. We hypothesized that BPs treatment modify the mineral and organic components of the newly-formed bone in craniofacial bone region. The aim of the study was thus to determine the ZA effects on bone material properties within the repaired bone defect area in the rat model. We proposed to examine the alterations of the newly-formed bone by Raman microspectroscopy and quantitative backscattered electron imaging (qBEI). In particular, we studied the relative gain/loss of newly-formed bone in ZA-treated rats with low ZA doses (i.e., those used for treating osteoporosis) or high ZA doses (i.e., those used for treating malignant bone diseases).

2. Materials and methods

2.1. Animals

Eighty adult male Sprague Dawley rats aged 56-day-old (400 g ± 20 g) were purchased from Elevage Janvier (Le Genest-Saint-Isles, France). All animals were housed individually in light- and temperature-controlled facilities and maintain with ad libitum access to a standard laboratory diet and water. All animals and surgical procedures were approved by the Veterinary Department of the French Ministry of Agriculture (approval no. 59-350137). The animals were treated in accordance with the guidelines of the Hospitalo-Universitary Department of Experimental Research of Lille (DHURE) and the Guide for Care and Use of Laboratory Animals (NIH publication 93-23).

2.2. Surgical procedure

Surgical procedures were performed under ketamine (50 mg/kg, Imalgen®) and xylasin (5 mg/kg, Rompun®). A dose of carprofen (15 mg/kg, Rimaldyl®) was administrated to control postoperative pain. After aseptic preparation, a semilunar incision was made through the skin and periosteum at the top of the *calvarium*, allowing reflection of a full thickness flap in posterior direction. A custom-made surgical guide was placed on the bone and fixed using two micro screws (0.9 × 1.3 mm Modus®, Mediartis S.A.R.L., Vaulx Milieu, France). A 4-mm diameter defect was made on sagittal suture with a trephine (Stoma®, Emmingen-Liptingen, Germany) using a low-speed handpiece under sterile saline irrigation. The surgical guide was removed and the micro screws were left as references to allow localization of the original margins of the surgical defect after bone healing. The soft tissues were then repositioned and sutured to achieve primary closure (4-0 threads Vicryl Ethicon®, Norderstedt, Germany). All animals exhibited normal activity and showed an increase in weight after surgery.

2.3. Dosing regimens

Zoledronic acid (ZA; 2-(imidazole-1-yl)-hydroxy-ethylidene-1, 1-bisphosphonic acid, disodium salt, 4.75 hydrate) was provided by Novartis Pharma (Basel, Switzerland). The drug was first dissolved in sterile physiological saline (0.9% NaCl) at a concentration of 50 μg/mL and then further diluted to the given concentration to be administrated for each animal.

Two weeks after surgery, animals were randomly treated with subcutaneous dose of vehicle (sterile physiological saline, 0.9%) or ZA following the same protocol. The randomization schedule was generated by an online statistical computing web programming (www.randomization.com).

Three doses of ZA were used as follows (Fig. 1):

- group ZA-S120 (n = 10): one single dose of 120 μg/kg body weight (equivalent to human osteoporosis treatment [27]);
- group ZA-M120 (n = 15): a daily dose of 20 μg/kg body weight for 6 days (either the fractionated of 120 μg/kg dosage);
- group ZA-M600 (n = 15): one weekly dose of 100 μg/kg body weight for 6 weeks (equivalent to 6 months of human bone metastasis treatment [28,29]).

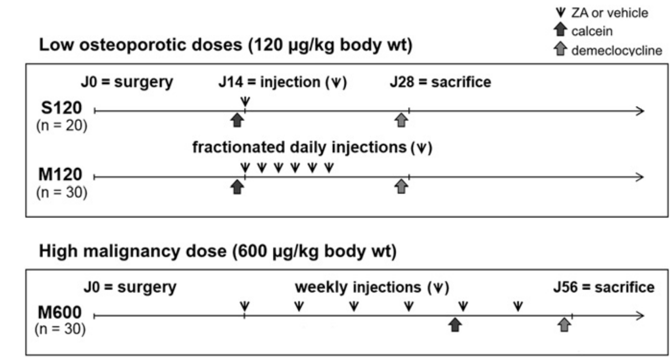

Fig. 1. Time-line diagram of injections procedures according the dosing regimen (low doses of 120 μg/kg body wt. or high dose of 600 μg/kg body wt.) and the administration rhythm (single, S or multiple, M injections). Two weeks after surgery, among each group S120, M120 and M600, an equivalent number of animals received randomly zoledronic acid (ZA) or vehicle. Additionally, animals received injections of 30 mg/kg body wt. calcein and demeclocycline at 15 days and 1 day before sacrifice respectively.

Similarly, a same number of animals were treated with vehicle to provide the respective control groups: CTL-S120 (n = 10), CTL-M120 (n = 15) and CTL-M600 (n = 15) groups.

To identify the newly-formed bone area, a double labelling was performed for which animals received intraperitoneally injections of calcein and demeclocycline (30 mg/kg body weight, Sigma-Aldrich®, Saint-Quentin Fallavier, France) at 15 days and 1 day before sacrifice respectively.

2.4. Tissue processing

At 4 weeks post-operation (groups S120 and M120) or 8 weeks post-operation (group M600), animals were sacrificed by lethal intracardiac injection of T61 under general sedation. The complete *calvarium* area was harvested and fixed in 70% ethanol solution for 48 h. Samples were embedded in poly-methyl methacrylate (PMMA). A 100-μm-thick section were cut in the cranio-caudal plane and progressively polished with silicium carbides and diamond suspension (Escil®, Chavassieu, France).

2.5. Selection of the bone areas

Imaging of fluorescence labelling was performed with an epifluorescence confocal microscope Zeiss LSM710 (Carl Zeiss, France) and the associated Zen 2009 software. The microscope was equipped with an Apochromat objective (×40, NA = 1.2), a multiline argon laser, and adequate filter blocks. For each sample, the acquisition of the entire *calvarium* bone section was performed to identify the newly-formed bone (defect bone area) from the native bone (distant bone areas). In the defect bone area, three distinct sampling areas were selected between the two fluorescent labelling (Fig. 2A). In some cases (3/80 animals), the signal of demeclocycline labelling was very low. In these cases, for which only calcein label was clearly discernible, the sampling areas were chosen in the calcein labelling area because we previously demonstrated that fluorescence did not affect the bone quality parameters [30]. In the distant area, three distinct sampling areas without fluorescent labelling were chosen to achieve comparison (Fig. 2B). For each sample, the quantitative backscattered electron

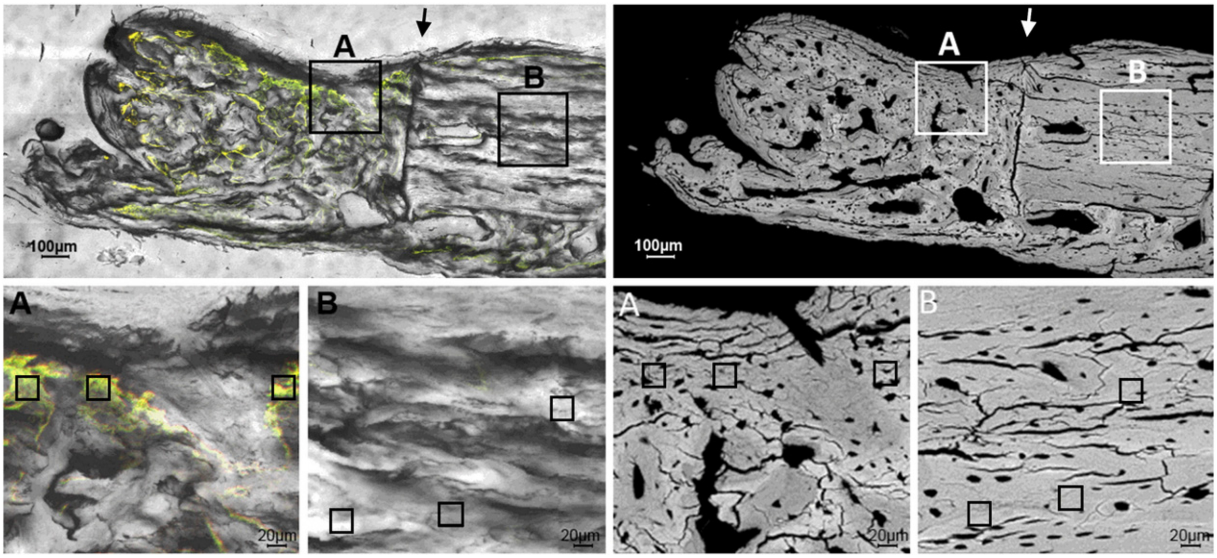

Fig. 2. Selection of the two bone areas of interest within the defect bone and the distant bone with epifluorescent imaging (left) and BE imaging (right). The demarcation between the defect bone area and the distant bone area is indicated by an arrow on the top images. To explain the choice of sampling areas for the analysis and the transposition, two large areas (A) and (B) were selected respectively within the defect bone and the distant bone (bottom images). On the left, the double fluorescent labels allowed the identification of three distinct sampling areas within the newly-formed bone in the defect bone area and the selection of three distinct sampling areas within the native bone without fluorescent labelling in the distant bone. On the right, figures showing the transposition of these bone sampling areas to BE images. For each sample, both the qBEI and Raman measurements were realized in the identical bone zones.

imaging (qBEI) and Raman measurements were performed in the same bone areas.

2.6. Quantitative backscattered electron imaging (qBEI)

Bone mineralization density distributions (BMDD) of the entire *calvarium* bone sections was determined using qBEI as previously described [31]. Briefly, samples were previously carbon coated under vacuum evaporation. A Scanning Electron Microscopy (Quanta 200 FEI) coupled with an Energy Dispersive X-rays analysis detector (EDS, QuanTax Bruker) was used. The accelerating voltage of the electron beam was adjusted to 20 kV and the working distance at 10 mm. A $\times$400 nominal magnification, corresponding to a pixel resolution of 1 µm/pixel was used. The digital backscattered electron (BE) image, consisting of 512 $\times$ 512 pixels, was generated by one single frame. Six digital BE images per sample (three localizations from the newly-formed bone and three localizations from the native bone) were taken and used for the BMDD evaluation. The digital BE images were analyzed by Aphelion software (ACDIS, Hérouville, France). A Region of Interest (ROI) of 25 $\times$ 25 µm was selected per BE images (Fig. 2). The gray-level histogram was extracted from the ROI. The BE gray-scale was calibrated using the "atomic number (Z) contrast" of reference materials [31]. The BE gray-scale was calibrated by changing brightness and contrast using PMMA resin (Z = 6), aluminium (Al, Z = 13), magnesium fluoride (MgF_2, Z_{mean} = 10) and tricalcium phosphate (β-TCP, Z_{mean} = 14.04). The experimental gray-levels of PMMA and β-TCP were taken as 0% and 38.7% of weight of calcium, respectively. The BE gray-level was converted into weight concentration calcium. This is the weight calcium concentration per percentage of bone areas of the scanned bone section that is defined as the BMDD [31]. The qBEI method is an indirect quantitative method to visualize relative changes of the local mineral concentration. In the bone tissue, the concentration of calcium, the constituent with the highest atomic number (Z = 20), dominantly influences the intensity of the BE gray-level. The contribution of other elements within the organic matrix (H, C, N, O, P, S) or within the mineral (P, O, H, C, Mg) can affect the BE signal but, in the mature bone, their contribution is considered to be negligible, as that was stated in previous studies [31,32].

Three variables, obtained from BMDD, reflecting the calcium distribution were studied [31]:

1. Ca_{Mean}, the average mean Ca concentration of mineralized bone,
2. $Ca_{MaxFreq}$, the peak height of the BMDD showing the maximal portion of bone area having an identical Ca concentration,
3. Ca_{Width}, the full width at half maximum of the distribution, reflecting the heterogeneity of mineralization density.

2.7. Raman microspectroscopy

Raman analyses were carried out on a Labram HR800 microspectrometer (Horiba Gr, Jobin Yvon, Lille, France) as described in a previous work [33]. Briefly, the spectrometer was equipped with a diode laser (λ = 785 nm), an air-cooled CDD (1024 $\times$ 256 pixels) and a $\times$100 objective (NA = 0.90, Olympus, France). The illumination spot size was close to 1 µm. Spectral acquisitions were done in the 300–1700 cm^{-1} range. The total acquisition time for each spectrum was 1 min with an integration time of 30 s and 2 accumulations. Each spectrum was treated with smoothing filtering (filter width: 5; and polynomial order: 2), and polynomial baseline correction (degree 4) with Labspec software (Horiba GR, Jobin Yvon, Lille, France).

Raman analyses were done prior to qBEI analyses to prevent artefacts due to carbon coating. The analyses were performed in newly-formed bone and in native bone for each sample. Point by point analyses were performed with a step of 5 µm and delimited by a square of 25 $\times$ 25 µm. This procedure was repeated 3 times per bone areas (three distinct localizations from the newly-formed bone and three distinct localizations from the native bone), and with a correspondence with the bone localizations of epifluorescence imaging and qBEI analyses. A total of 150 spectra were obtained per sample.

All data analyses were performed using Matlab R2010a (Mathworks, Inc., Natick, MA, USA). Five physicochemical variables were determined from Raman spectra [34]:

1. The mineral-to-organic ratio = intensity ratio between ν_1 PO_4 (960 cm^{-1}) to the $\delta(CH_2)$ side-chains of collagen molecules (1450 cm^{-1}) bands. The mineral to organic ratio reflects the relative amount of mineral par amount of organic matrix and described the mineral content of bone;

2. The monohydrogen phosphate content = intensity ratio between ν_3 HPO_4 (1003 cm^{-1}) and ν_1 PO_4 bands. The monohydrogen phosphate (HPO_4) content reflects the conversion of nonapatitic precursors into apatitic mineral and consequently is related to the mineral bone maturity;
3. The crystallinity = inverse of the full width at half maximum intensity (FWHM) of the $\nu_1 PO_4$ band. The crystallinity reflects mineral crystal size and perfection; this is increased during mineralization from initial amorphous calcium phosphate phases to well-ordered apatite forms.
4. The type-B carbonate substitution = intensity ratio between B-type CO_3 (1071 cm^{-1}) and ν_1 PO_4 bands. This non-stoichiometric substitution of PO_4 ions in the crystal lattice (called type-B substitution) promotes structural changes occurring within the crystal lattice (vacancies, shape and symmetry changes of the mineral crystal).
5. The hydroxyproline-to-proline ratio = intensity ratio between proline (855 cm^{-1}) and hydroxyproline bands (870 cm^{-1}). The hydroxyproline-to-proline ratio gives an assessment of the collagen posttranslational modifications. The hydroxyproline-to-proline ratio had been suggested to be linked with the mineralization pattern [35].

These physicochemical variables are linked to pathophysiological behavior of bone. In addition, relationships between these physicochemical variables and the biomechanical properties have been recently investigated and described [36–38].

2.8. Data expression

To overcome the individual variations, the relative gain/loss of each variable was assessed in the newly-formed bone in comparison with the distant bone. For each animal, the variable's raw average in the newly-formed bone was weighted by the variable's raw average in the distant bone as follow:

$$x = \frac{\text{MEAN defect} - \text{MEAN distant}}{\text{MEAN distant}}.$$

This relative gain/loss values matches with x-fold the raw value of the distant bone taken as baseline.

2.9. Statistical analysis

For each animal, the x value of relative gain/loss for each variable was treated as a single statistical unit. Data are presented as mean ± standard deviation (SD). Due to the importance of relative values interanimal variability, non-parametric tests were done. Difference between ZA and CTL groups for each S120, M120 and M600 conditions, was tested using a Mann-Whitney *U* test. Correlation between variables was examined among each group by linear regression and Spearman's ρ rank correlation coefficient calculated. Statistical significance was assigned to $P < 0.05$.

3. Results

3.1. Bone mineral calcium concentration in newly-formed bone

The average mean Ca concentration (Ca_{Mean}) was unchanged between the ZA groups and their respective CTL groups in any S120, M120 and M600 conditions (Table 1).

The maximal portion of bone area having an identical Ca concentration ($Ca_{MaxFreq}$) was similar between the ZA groups and their respective CTL groups in any S120, M120 and M600 conditions (Table 1).

No difference was observed in the heterogeneity of mineralization density (Ca_{Width}) for the three ZA groups in comparison to their respective CTL groups (Table 1).

3.2. Bone mineral and collagenic composition/organization in newly-formed bone

Several modifications of the bone mineral and collagen variables have been previously demonstrated during bone formation processes according to the tissue age of the newly-formed bone [36,39]. As expected, we observed significant modifications of different variables of the newly-formed bone during healing processes between the CTL-M600 group (28 days post-surgery) versus both CTL-S120 and CTL-M120 groups (56 days post-surgery) as follows: a decrease of the relative value of type-B carbonate substitution and of the HPO_4 content, and an increase of the relative value of crystallinity and of the hydroxyproline-to-proline ratio (data not shown). For that reason, comparisons were done between a ZA group and its respective CTL group.

No difference was observed in the mineral content, neither the mineral-to-organic ratio nor the HPO_4 content, for the three ZA groups in comparison to their respective CTL groups (Table 1).

In the ZA-M600 group, a significant decrease of the relative value of crystallinity (−25%, P = 0.0298) was observed, when compared to the respective CTL-M600 group (Fig. 3). Additionally, a significant decrease of the relative value of the hydroxyproline-to-proline ratio

Table 1
Study of the relative Raman and qBEI variables from newly-formed bone in rat calvaria area for the three ZA groups and their respective controls (Mann-Whitney *U* test).

	S120		M120		M600	
	CTL (n = 10/20)	ZA (n = 10/20)	CTL (n = 15/30)	ZA (n = 15/30)	CTL (n = 15/30)	ZA (n = 15/30)
Mineral-to-organic ratio[a]	0.142 ± 0.143	0.216 ± 0.142	0.046 ± 0.126	−0.056 ± 0.095	−0.002 ± 0.113	0.045 ± 0.128
Crystallinity[b]	−0.030 ± 0.018	−0.046 ± 0.022	−0.022 ± 0.041	−0.050 ± 0.018	0.495 ± 0.213	**0.369 ± 0.088***
Type-B CO_3 substitution[c]	−0.013 ± 0.037	−0.036 ± 0.045	−0.024 ± 0.035	−0.042 ± 0.038	−0.164 ± 0.080	−0.111 ± 0.072
HPO_4 content[d]	0.160 ± 0.142	0.064 ± 0.114	0.227 ± 0.166	0.217 ± 0.159	−0.032 ± 0.047	−0.023 ± 0.028
OHpro-to-pro ratio[e]	0.015 ± 0.052	0.013 ± 0.021	−0.016 ± 0.039	−0.029 ± 0.059	0.400 ± 0.239	**0.279 ± 0.083****
Ca_{Mean}[f]	0.099 ± 0.045	0.133 ± 0.034	0.084 ± 0.034	0.071 ± 0.047	0.132 ± 0.035	0.151 ± 0.041
$Ca_{MaxFreq}$[g]	0.028 ± 0.061	0.019 ± 0.071	0.078 ± 0.070	0.065 ± 0.059	0.183 ± 0.142	0.192 ± 0.093
Ca_{Width}[h]	−0.061 ± 0.076	−0.037 ± 0.073	−0.056 ± 0.092	−0.074 ± 0.100	−0.021 ± 0.118	−0.023 ± 0.089

The relative gain was expressed as a positive value, and the relative loss as a negative value which matches with x-fold the raw value of distant bone. The mean ± SD are listed. The statistical significance between ZA groups and their respective CTL groups is denoted by bold text.
*P = 0.0298 and **P = 0.0247, compared to CTL.
[a] Mineral-to-organic ratio = υ_1 (PO_4)/δ(CH_2)-wag.
[b] Crystallinity = 1/FWHM de υ_1 (PO_4).
[c] Type-B CO_3 substitution = υ_1 (CO_3)/υ_1 (PO_4) bands.
[d] HPO_4 content = ν_3 HPO_4^{2-}/υ_1 (PO_4) bands.
[e] OHpro-to-pro ratio = hydroxyproline/proline ratio.
[f] Ca_{mean} = the average mean calcium concentration.
[g] $Ca_{MaxFreq}$ = the maximal portion of bone area having an identical calcium concentration.
[h] Ca_{width} = the heterogeneity of mineralization density.

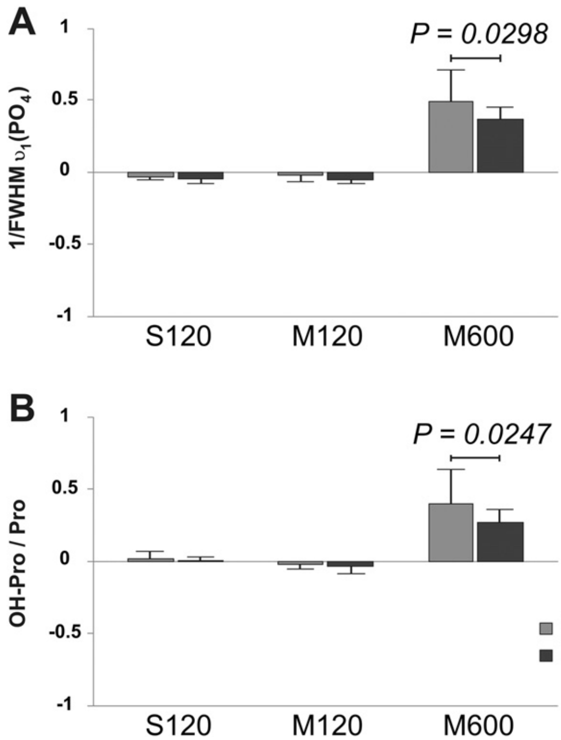

Fig. 3. Comparison of the relative gain/loss of variables in the newly-formed bone according to the dosing regimen (S120, M120, and M600) between ZA groups and its corresponding CTL groups: relative values of crystallinity (A) and hydroxyproline-to-proline ratio (B).

(-30%, $P = 0.0247$) was observed, when compared to the respective CTL-M600 group (Fig. 3).

These variables were unchanged in the ZA-S120 and ZA-M120 groups, compared to their respective CTL-S120 and CTL-M120 groups (Fig. 3).

3.3. Potential correlations between the different variables

Correlations between the relative variables are indicated in Table 2.

For both M600 CTL- and ZA-groups, the crystallinity was positively correlated with the hydroxyproline-to-proline ratio ($\rho = 0.80$ and 0.90 respectively, $P < 0.0005$) (Fig. 4A), and the mineral-to-organic ratio negatively correlated with the HPO_4 content ($\rho = -0.58$ and -0.51 respectively, $P < 0.05$) (Fig. 4B).

Other correlations were observed either only in a CTL group or only in a ZA group, which we consider as minor correlations. No other major correlation between variables was observed in both ZA and CTL groups.

4. Discussion

Bone quality, especially intrinsic bone material properties of the newly-formed bone was evaluated by qBEI and Raman variables within bone defect of rat's *calvaria*. The newly-formed bone at the same tissue age was determined by the double labelling technique using two distinct cyclines to compare ZA group with the corresponding CTL group for each dosing regimen. As healing could differ between each individual, ZA effects were studied on relative gain/loss parameters to assess the newly-formed bone quality within a bone defect repaired area.

Apatite crystal organization is defined as the perfection and relative size/strain of the crystal and is determined by the crystallinity [40]. In the present study, the crystallinity decreased in the ZA-M600 compared to the CTL-M600 group, suggesting that high ZA doses should be involved in the crystal lattice rearrangement of newly-formed bone. Our results agree with previous observations made in actively bone-forming surface of trabecular bone in ZA-treated osteoporotic women after 3-years treatments [18,19]. This effect was suggested to be attributed to ZA, which could alter the osteoblastic function and/or the rate of mineral maturation [18,19]. Interestingly in the present study, no variation was observed on mineral components (Ca or PO_4) or on mineral maturity determined by the HPO_4 content. For the same age of newly-formed bone tissue, our results preclude that ZA does not act on bone mineral apposition or maturation, but can change the apatite organization. Due to the ZA negative zeta potential at pH 7.4, its adsorption into the apatite crystal was reported to modify the crystal electrical charge and to increase potential attractions to ionic and/or matrix mineralization molecules and, thus to reorganize the crystalline growth [41,42]. Another hypothesis of changes in the crystalline organization could be an ionic substitution of the ZA molecule among apatite crystal lattice [43]. The ZA uptake in biological apatite possibly causes such early molecular restructuring and disruption on apatite crystal lattice during its growth.

The hydroxyproline-to-proline ratio was use to investigate the intrachain collagen stability. Indeed, in the nascent collagen fibril, some proline moieties can be hydroxylated to further stabilize the collagen helical structure by intrachain hydrogen bounds [44,45]. Fibrils in which proline moieties have not been hydroxylated are far less stable than fibers in which these moieties have been hydroxylated [46]. The use of the hydroxyproline and proline bands taken together was recently suggested as reliable collagen markers for Raman analyses [47]. The authors assume that the sum of proline and hydroxyproline is constant while the ratio of these two variables fluctuates in function of the proline hydroxylation rate [42]. In the present study, the hydroxyproline-to-proline ratio was decreased in the ZA-M600 group compared to the CTL-M600 group, indicating a reduction of proline hydroxylation and consequently a reduction of the intrachain collagen stability. Other collagen posttranslationnal modifications about interfibril collagen cross-linking (that reflects the collagen maturity) have been previously reported with various BPs treatment [48–53]. Due a long-term suppression of bone remodeling, long-term BPs treatments were linked to an increase of the collagen maturity [48–51]. Yet, in actively bone forming surfaces based on fluorescent labelling, the collagen maturity varied according to the BPs and independently to the bone remodeling [52, 53]. In the present study, the collagen posttranslational modifications about the proline hydroxylation similarly indicated an effect of high ZA doses during bone formation and independently to its bone remodeling suppression. The proline hydroxylation occurs earlier than the cross-linking and, in the endoplasmic reticulum of osteoblasts [44,45]. In a similar rat *calvarial* bone defect model, the collagen production by osteoblasts was shown to be highest at the second week after bone defect surgery [21] coinciding in our model with the first ZA injection. Previous data indicated that small amount of BPs could be internalized by osteoblasts [54]. The BPs effects on osteoblastic cells and their implications on collagen [55–58] and mineral production [59–61] are still debated. To date, the roles of BPs on osteoblasts could not be established in vivo and it is difficult according to the coupling between osteoclasts and osteoblasts to highlight such indirect effects on remodeling cycle. In the present study, alterations of the hydroxyproline-to-proline ratio seem to indicate a potential effect of ZA on osteoblasts during bone formation.

Interestingly, we found that, in the older rats and independently of the treatment without or with ZA (M600), the crystallinity was positively correlated with the hydroxyproline-to-proline ratio. Collagen posttranslational modifications were reported to be implicated in mineralization pattern depending to species [35] and in mineralization mechanism in brittle bone diseases [62]. During bone formation, the hierarchical structure of collagen fibers provides a scaffold for ordering apatite mineral deposition [63] and could also modify the crystallinity. The hydroxyproline promotes stronger interactions to hydroxyapatite surface than proline due to its extra hydroxy functional group [64]. Thus, hydroxylation of the proline could act on early collagen

Table 2
Study of potential correlations between the different variables for each rat group. The Spearman's ρ values and (the P value) are listed.

			Ca_{Mean}[f]	$Ca_{MaxFreq}$[g]	Ca_{Width}[h]	OHpro-to-pro ratio[e]	HPO_4 content[d]	Type-B CO_3 substitution[c]	Crystallinity[b]
Mineral-to-organic ratio[a]	S120	CTL	0.28 (0.425)	−0.44 (0.200)	0.19 (0.603)	**0.73 (0.016)**	−0.45 (0.187)	**0.64 (0.048)**	0.32 (0.365)
		ZA	−0.57 (0.082)	**−0.72 (0.019)**	−0.02 (0.960)	−0.19 (0.603)	0.22 (0.533)	0.03 (0.934)	0.22 (0.533)
	M120	CTL	−0.06 (0.830)	−0.20 (0.467)	−0.08 (0.771)	0.25 (0.376)	−0.36 (0.191)	0.25 (0.362)	−0.05 (0.869)
		ZA	0.08 (0.761)	−0.14 (0.625)	−0.25 (0.367)	0.19 (0.499)	−0.05 (0.850)	0.35 (0.196)	0.12 (0.671)
	M600	CTL	−0.07 (0.855)	−0.43 (0.214)	0.41 (0.244)	0.02 (0.940)	**−0.58 (0.031)**	0.425 (0.114)	−0.11 (0.685)
		ZA	**0.72 (0.005)**	0.40 (0.174)	−0.12 (0.694)	−0.5 (0.859)	**−0.51 (0.050)**	0.30 (0.283)	0.02 (0.929)
Crystallinity[b]	S120	CTL	0.55 (0.98)	0.09 (0.803)	0.11 (0.751)	0.11 (0.751)	−0.56 (0.090)	0.48 (0.161)	
		ZA	0.03 (0.934)	−0.15 (0.676)	0.31 (0.385)	0.39 (0.260)	0.01 (0.987)	**0.68 (0.029)**	
	M120	CTL	0.16 (0576)	−0.13 (0.639)	−0.06 (0.830)	0.18 (0.507)	0.11 (0.685)	0.12 (0.666)	
		ZA	0.46 (0.084)	**−0.65 (0.008)**	0.19 (0.495)	**−0.54 (0.037)**	−0.33 (0.223)	0.09 (0.747)	
	M600	CTL	0.17 (0.627)	−0.02 (0.960)	0.13 (0.726)	**0.80 (0.0003)**	0.22 (0.435)	−0.19 (0.499)	
		ZA	−0.01 (0.972)	−0.09 (0.761)	0.29 (0.334)	**0.90 (<0.0001)**	−0.33 (0.22)	0.11 (0.704)	
Type-B CO_3 substitution[c]	S120	CTL	0.20 (0.580)	−0.07 (0.855)	0.48 (0.161)	0.48 (0.161)	−0.61 (0.060)		
		ZA	0.16 (0.651)	−0.03 (0.934)	−0.01 (0.987)	0.56 (0.090)	−0.15 (0.676)		
	M120	CTL	0.09 (0.742)	−0.30 (0.271)	0.16 (0.576)	0.26 (0.355)	0.00 (1.000)		
		ZA	−0.02 (0.93)	0.21 (0.450)	0.23 (0.413)	0.22 (0.420)	−0.23 (0.398)		
	M600	CTL	0.24 (0.511)	0.28 (0.425)	0.01 (0.990)	0.06 (0.840)	0.05 (0.869)		
		ZA	0.52 (0.071)	0.10 (0.748)	−0.17 (0.578)	0.06 (0.830)	**−0.72 (0.002)**		
HPO_4 content[d]	S120	CTL	**−0.77 (0.009)**	0.11 (0.751)	0.15 (0.676)	−0.55 (0.098)			
		ZA	0.42 (0.229)	0.37 (0.293)	−0.38 (0.276)	−0.03 (0.934)			
	M120	CTL	−0.42 (0.121)	0.29 (0.296)	−0.08 (0.771)	−0.08 (0.761)			
		ZA	−0.08 (0.761)	0.01 (0.980)	0.04 (0.889)	0.06 (0.830)			
	M600	CTL	0.59 (0.074)	0.59 (0.073)	−0.11 (0.751)	0.36 (0.191)			
		ZA	−0.33 (0.271)	0.03 (0.929)	−0.17 (0.578)	−0.23 (0.405)			
OHpro-to-pro ratio[e]	S120	CTL	0.32 (0.365)	**−0.67 (0.033)**	0.10 (0.777)				
		ZA	0.16 (0.651)	0.36 (0.310)	0.07 (0.855)				
	M120	CTL	0.05 (0.850)	0.23 (0.413)	−0.10 (0.732)				
		ZA	−0.05 (0.850)	0.37 (0.170)	−0.25 (0.369)				
	M600	CTL	0.54 (0.108)	0.20 (0.580)	−0.16 (0.651)				
		ZA	0.08 (0.803)	0.38 (0.194)	0.33 (0.271)				

The relative gain was expressed as a positive value, and the relative loss as a negative value which matches with *x*-fold the raw value of distant bone. The mean ± SD are listed. The statistical significance between ZA groups and their respective CTL groups is denoted by bold text.
[a] Mineral-to-organic ratio = υ_1 (PO_4)/δ(CH_2)-wag.
[b] Crystallinity = 1/FWHM de υ_1 (PO_4).
[c] Type-B CO_3 substitution = υ_1 (CO_3)/υ_1 (PO_4) bands.
[d] HPO_4 content = ν_3 HPO_4^{2-}/υ_1 (PO_4) bands.
[e] OHpro-to-pro ratio[e] = hydroxyproline/proline ratio.
[f] Ca_{mean} = the average mean calcium concentration.
[g] $Ca_{MaxFreq}$ = the maximal portion of bone area having an identical calcium concentration.
[h] Ca_{width} = the heterogeneity of mineralization density.

organization and possibly promote apatite crystal growth and order on the collagen matrix.

In the present study, no variation in the local mineral concentration was observed at any ZA dose level tested. In the mature bone, the correlation between qBEI measurements and mineral content [32,65] and the qBEI measurements underline dominantly the concentration of calcium. The contribution of other elements (C, O, P) within organic or mineral bone matrix is considered to be negligible as stated in previous studies [31,32]. In the newly-formed bone (identified by the double labelling technique), the correlation between qBEI measurements and mineral content is not clearly established. It cannot be excluded that the local contribution of other elements (C, O, P) from bone matrix or embedding material component may influence the qBEI measurements. Due to these limitations, the qBEI measurements need to be carefully considered in the newly-formed bone to determinate the relative changes of local mineral concentration occurred [65].

Furthermore, only the influence of ZA on newly-formed bone is investigated. Long-term consequences on bone quality (i.e. composition and structure), especially some disturbance or some failure of the newly-formed bone's remodeling, is possible with ZA administration. If the rodent *calvarial* bone defect is a well-established model to carry out the bone formation processes [20–26], such long-term bone remodeling evaluation is difficult with the rodent due to its lack of bone remodeling [66]. The alterations of apatite organization and collagen stability are observed with high ZA doses (ZA-M600 group); no difference was observed with the lower dose of ZA (neither ZA-S120 nor ZA-M120 groups). Nevertheless, the impact of the ZA larger dose cannot be dissociated from the longer time period between the ZA-M600 group and the ZA-S120 or ZA-M120 groups and have to be considered. In the present study, we care to be clinically relevant to bone malignancy treatment with a weekly dose of 100 μg/kg [28,29]. Indeed, in human treatment, the nephrotoxicity is a well-known side effect of bisphosphonates. Some cases of renal toxicity have been previously documented following zoledronic acid treatment in patients with malignancy diseases [67–71]. According to bisphosphonate treatment recommendations, zoledronic acid is given at a 4 mg-dose every 3 or 4 weeks for the bone malignancy treatment to prevent side effects [72]. In rat, due to the long half-life of zoledronic acid in renal tissue and its complete renal clearance observed with at least 96 h [73], a daily administration would induce a renal toxicity. The design of the present study has been determined to mimic the safety of this malignancy dosage and administration. In addition, the timing of repeated ZA injections with the high dose cannot be dissociated from the dosing regimen and have also to be considered. There are some key moments in the bone formation process that will determine the effects of ZA administration: in similar bone defect even if mineral apposition increases gradually with time up to 8 weeks of bone healing process [22], the osteoblastic collagen matrix producing is highest at 2 weeks [21], and the bone mineral deposition is highest at 4 weeks [20]. In the present study, an efficient dose of ZA delivered during these key strategic moments seems to modify the collagen matrix organization and the newly-formed mineral crystals structure during their deposit.

In summary, the present study focuses on the short-term influence of ZA on mineral and organic components into a bone defect healing in the rat model. Our findings highlight some new properties for high ZA doses on newly-formed bone in a craniofacial defect model without

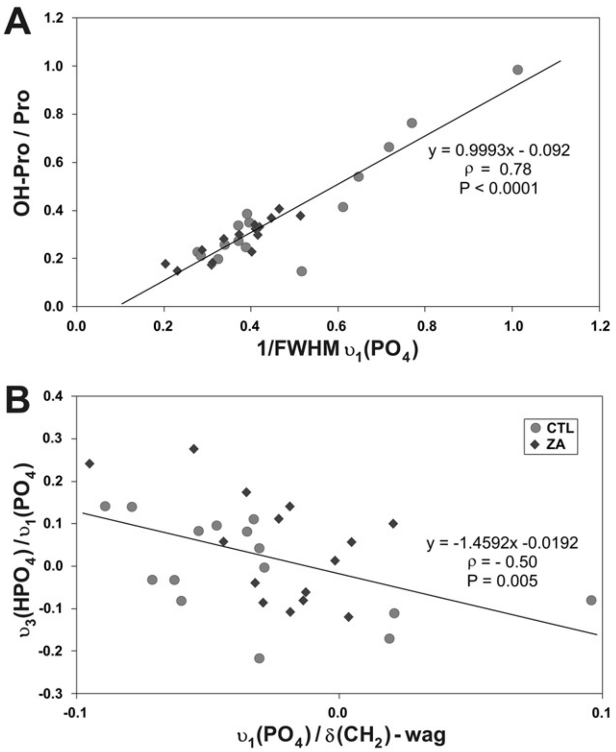

Fig. 4. Correlations between the relative values of the crystallinity and the hydroxyproline-to-proline ratio (A), and between the mineral-to-organic ratio and the HPO_4 content (B) among both M600 groups. Full diamond and empty circle represent the M600-ZA group and the M600-CTL group, respectively.

functional stimulation. Contrarily to high ZA doses, which are equivalent to 6 months of human bone metastasis treatment, the intrinsic bone material properties of the newly-formed bone weren't modified by neither single nor fractionated low ZA doses, which are equivalent to human osteoporosis treatment. As already reported for bone remodeling, here we found that the apatite crystal organization during the bone healing process was disrupted by high ZA doses. Additionally, we reported for the first time that the intrachain collagen stability was reduced by high ZA doses, as reflected by the decrease of the hydroxyproline-to-proline ratio. These altered collagen modifications suggest that ZA may affect the osteoblast functions during early stages of bone repair in the rat model. Additional studies are required to explore the BPs influence in humans on the early collagen organization, especially at actively bone-forming surfaces.

Conflict of interest

BC consults for and/or receives honoraria for research programs or investigator fees from Amgen, Daiichi-Sankyo, Ferring, GSK, Lilly, MSD, Medtronic, Novartis, Servier, and Roche.

All other authors have nothing to declare.

Acknowledgments

The authors thank the staff of the Hospitalo-Universitary Department of Experimental Research (DHURE), Lille, France, for supplying the help on the surgical procedures. We also thank M. Tardivel of the University of Lille, France for her technical assistance and the fluorescence imaging facilities. We acknowledge Novartis Pharma for providing zoledronic acid for this study. We thank the Institut Français pour la Recherche Odontologique (IFRO) and the Société Française de Chirurgie Orale (SFCO) for their financial support.

References

[1] R.R. Recker, L. Armas, The effect of antiresorptives on bone quality, Clin. Orthop. Relat. Res. 469 (8) (Aug 2011) 2207–2214.
[2] E. Seeman, Bone morphology in response to alendronate as seen by high-resolution computed tomography: through a glass darkly, J. Bone Miner. Res. 25 (12) (Dec 2010) 2553–2557.
[3] A.J. Roelofs, C.A. Stewart, S. Sun, K.M. Błażewska, B.A. Kashemirov, C.E. McKenna, et al., Influence of bone affinity on the skeletal distribution of fluorescently labeled bisphosphonates in vivo, J. Bone Miner. Res. 27 (4) (2012) 835–847.
[4] K. Iwata, J. Li, H. Follet, R.J. Phipps, D.B. Burr, Bisphosphonates suppress periosteal osteoblast activity independently of resorption in rat femur and tibia, Bone 39 (5) (Nov 2006) 1053–1058.
[5] M. Kashii, J. Hashimoto, T. Nakano, Y. Umakoshi, H. Yoshikawa, Alendronate treatment promotes bone formation with a less anisotropic microstructure during intramembranous ossification in rats, J. Bone Miner. Metab. 26 (1) (2008) 24–33.
[6] A. Feher, A. Koivunemi, M. Koivunemi, R.K. Fuchs, D.B. Burr, R.J. Phipps, et al., Bisphosphonates do not inhibit periosteal bone formation in estrogen deficient animals and allow enhanced bone modeling in response to mechanical loading, Bone 46 (1) (Jan 2010) 203–207.
[7] N. Amanat, L.H. He, M.V. Swain, D.G. Little, The effect of zoledronic acid on the intrinsic material properties of healing bone: an indentation study, Med. Eng. Phys. 30 (7) (Sep 2008) 843–847.
[8] M.M. McDonald, S. Dulai, C. Godfrey, N. Amanat, T. Sztynda, D.G. Little, Bolus or weekly zoledronic acid administration does not delay endochondral fracture repair but weekly dosing enhances delays in hard callus remodeling, Bone 43 (4) (Oct 2008) 653–662.
[9] C. Acevedo, H. Bale, B. Gludovatz, A. Wat, S.Y. Tang, M. Wang, et al., Alendronate treatment alters bone tissues at multiple structural levels in healthy canine cortical bone, Bone 81 (Aug 5 2015) 352–363.
[10] S.S. Huja, A. Mason, C.E. Fenell, X. Mo, S. Hueni, A.M. D'Atri, et al., Effects of short-term zoledronic acid treatment on bone remodeling and healing at surgical sites in the maxilla and mandible of aged dogs, J. Oral Maxillofac. Surg. 69 (2) (Feb 2011) 418–427.
[11] F.P. Yamamoto-Silva, V. Bradaschia-Correa, L.A.P.A. Lima, V.E. Arana-Chavez, Ultrastructural and immunohistochemical study of early repair of alveolar sockets after the extraction of molars from alendronate-treated rats, Microsc. Res. Tech. 76 (6) (Jun 2013) 633–640.
[12] S. Kuroshima, R.B. Mecano, R. Tanoue, K. Koi, J. Yamashita, Distinctive tooth-extraction socket healing: bisphosphonate versus parathyroid hormone therapy, J. Periodontol. 85 (1) (Jan 2014) 24–33.
[13] R. Tanoue, K. Koi, J. Yamashita, Effect of alendronate on bone formation during tooth extraction wound healing, J. Dent. Res. 94 (9) (Jun 29 2015) 1251–1258.
[14] A.H.A. Kurth, C. Eberhardt, S. Müller, M. Steinacker, M. Schwarz, F. Bauss, The bisphosphonate ibandronate improves implant integration in osteopenic ovariectomized rats, Bone 37 (2) (Aug 2005) 204–210.
[15] J. Blazsek, C. Dobó Nagy, I. Blazsek, R. Varga, B. Vecsei, P. Fejérdy, et al., Aminobisphosphonate stimulates bone regeneration and enforces consolidation of titanium implant into a new rat caudal vertebrae model, Pathol. Oncol. Res. 15 (4) (Dec 2009) 567–577.
[16] J. Abtahi, P. Tengvall, P. Aspenberg, A bisphosphonate-coating improves the fixation of metal implants in human bone. A randomized trial of dental implants, Bone 50 (5) (May 2012) 1148–1151.
[17] C.-T. Leu, E. Luegmayr, L.P. Freedman, G.A. Rodan, A.A. Reszka, Relative binding affinities of bisphosphonates for human bone and relationship to antiresorptive efficacy, Bone 38 (5) (May 2006) 628–636.
[18] S. Gamsjaeger, B. Buchinger, E. Zwettler, R. Recker, D. Black, J.A. Gasser, et al., Bone material properties in actively bone-forming trabeculae in postmenopausal women with osteoporosis after three years of treatment with once-yearly zoledronic acid, J. Bone Miner. Res. 26 (1) (Jan 2011) 12–18.
[19] S. Gamsjaeger, B. Hofstetter, E. Zwettler, R. Recker, J.A. Gasser, E.F. Eriksen, et al., Effects of 3 years treatment with once-yearly zoledronic acid on the kinetics of bone matrix maturation in osteoporotic patients, Osteoporos. Int. 24 (1) (Jan 2013) 339–347.
[20] T. Honma, T. Itagaki, M. Nakamura, S. Kamakura, I. Takahashi, S. Echigo, et al., Bone formation in rat calvaria ceases within a limited period regardless of completion of defect repair, Oral Dis. 14 (5) (Jul 2008) 457–464.
[21] T. Itagaki, T. Honma, I. Takahashi, S. Echigo, Y. Sasano, Quantitative analysis and localization of mRNA transcripts of type I collagen, osteocalcin, MMP 2, MMP 8, and MMP 13 during bone healing in a rat calvarial experimental defect model, Anat. Rec. Hoboken 291 (8) (Aug 2008) 1038–1046.
[22] H. Okata, M. Nakamura, A. Henmi, S. Yamaguchi, Y. Mikami, H. Shimauchi, et al., Calcification during bone healing in a standardised rat calvarial defect assessed by micro-CT and SEM-EDX, Oral Dis. 21 (1) (Jan 2015) 74–82.
[23] M. Nagata, M. Messora, R. Okamoto, N. Campos, N. Pola, L. Esper, et al., Influence of the proportion of particulate autogenous bone graft/platelet-rich plasma on bone healing in critical-size defects: an immunohistochemical analysis in rat calvaria, Bone 45 (2) (Aug 2009) 339–345.
[24] S. Vigier, C. Catania, B. Baroukh, J.-L. Saffar, M.-M. Giraud-Guille, M.-L. Colombier, Dense fibrillar collagen matrices sustain osteoblast phenotype in vitro and promote bone formation in rat calvaria defect, Tissue Eng. A 17 (7–8) (Apr 2011) 889–898.
[25] W. Chen, J. Liu, N. Manuchehrabadi, M.D. Weir, Z. Zhu, H.H.K. Xu, Umbilical cord and bone marrow mesenchymal stem cell seeding on macroporous calcium phosphate for bone regeneration in rat cranial defects, Biomaterials 34 (38) (Dec 2013) 9917–9925.
[26] P.P. Spicer, J.D. Kretlow, S. Young, J.A. Jansen, F.K. Kasper, A.G. Mikos, Evaluation of bone regeneration using the rat critical size calvarial defect, Nat. Protoc. 7 (10) (Oct 2012) 1918–1929.

[27] E. Biver, M.H. Vieillard, B. Cortet, J. Salleron, G. Falgayrac, G. Penel, No anti-angiogenic effect of clinical dosing regimens of a single zoledronic acid injection in an experimental bone healing site, Bone 46 (3) (Mar 2010) 643–648.
[28] D. Heymann, B. Ory, F. Blanchard, M.-F. Heymann, P. Coipeau, C. Charrier, et al., Enhanced tumor regression and tissue repair when zoledronic acid is combined with ifosfamide in rat osteosarcoma, Bone 37 (1) (Jul 2005) 74–86.
[29] J. Yamashita, K. Koi, D.-Y. Yang, L.K. McCauley, Effect of zoledronate on oral wound healing in rats, Clin. Cancer Res. 17 (6) (Mar 15 2011) 1405–1414.
[30] C. Olejnik, G. Falgayrac, A. During, G. Penel, Compatibility of fluorochrome labeling protocol with Raman spectroscopy to study bone formation, Bull. Group. Int. Rech. Sci. Stomatol. Odontol. 50 (2) (2011) 34–36.
[31] P. Roschger, P. Fratzl, J. Eschberger, K. Klaushofer, Validation of quantitative backscattered electron imaging for the measurement of mineral density distribution in human bone biopsies, Bone 23 (4) (Oct 1998) 319–326.
[32] R.D. Bloebaum, J.G. Skedros, E.G. Vajda, K.N. Bachus, B.R. Constantz, Determining mineral content variations in bone using backscattered electron imaging, Bone 20 (5) (May 1997) 485–490.
[33] G. Falgayrac, B. Cortet, O. Devos, J. Barbillat, V. Pansini, A. Cotten, et al., Comparison of two-dimensional fast Raman imaging versus point-by-point acquisition mode for human bone characterization, Anal. Chem. 84 (21) (Nov 6 2012) 9116–9123.
[34] C. Olejnik, G. Falgayrac, A. During, M.H. Vieillard, J.M. Maes, B. Cortet, et al., Molecular alterations of bone quality in sequesters of bisphosphonates-related osteonecrosis of the jaws, Osteoporos. Int. 25 (2) (Feb 2014) 747–756.
[35] K. Buckley, P. Matousek, A.W. Parker, A.E. Goodship, Raman spectroscopy reveals differences in collagen secondary structure which relate to the levels of mineralisation in bones that have evolved for different functions, J. Raman Spectrosc. 43 (9) (2012) 1237–1243.
[36] E. Donnelly, A.L. Boskey, S.P. Baker, M.C.H. van der Meulen, Effects of tissue age on bone tissue material composition and nanomechanical properties in the rat cortex, J. Biomed. Mater. Res. A 92 (3) (2010 Mar) 1048–1056.
[37] X. Bi, C.A. Patil, C.C. Lynch, G.M. Pharr, A. Mahadevan-Jansen, J.S. Nyman, Raman and mechanical properties correlate at whole bone- and tissue-levels in a genetic mouse model, J. Biomech. 44 (2) (Jan 11 2011) 297–303.
[38] G.S. Mandair, M.D. Morris, Contributions of Raman spectroscopy to the understanding of bone strength, BoneKEy Rep. 4 (2015) 620.
[39] C.P. Tarnowski, M.A. Ignelzi Jr., M.D. Morris, Mineralization of developing mouse calvaria as revealed by Raman microspectroscopy, J. Bone Miner. Res. 17 (6) (Jun 2002) 1118–1126.
[40] J.S. Yerramshetty, C. Lind, O. Akkus, The compositional and physicochemical homogeneity of male femoral cortex increases after the sixth decade, Bone 39 (6) (Dec 2006) 1236–1243.
[41] R.G.G. Russell, N.B. Watts, F.H. Ebetino, M.J. Rogers, Mechanisms of action of bisphosphonates: similarities and differences and their potential influence on clinical efficacy, Osteoporos. Int. 19 (6) (Jun 1 2008) 733–759.
[42] G.H. Nancollas, R. Tang, R.J. Phipps, Z. Henneman, S. Gulde, W. Wu, et al., Novel insights into actions of bisphosphonates on bone: differences in interactions with hydroxyapatite, Bone 38 (5) (May 2006) 617–627.
[43] A. Juillard, G. Falgayrac, B. Cortet, M.-H. Vieillard, N. Azaroual, J.-C. Hornez, et al., Molecular interactions between zoledronic acid and bone: an in vitro Raman microspectroscopic study, Bone 47 (5) (Nov 2010) 895–904.
[44] S.M. Krane, The importance of proline residues in the structure, stability and susceptibility to proteolytic degradation of collagens, Amino Acids 35 (4) (Nov 2008) 703–710.
[45] S. Viguet-Carrin, P. Garnero, P.D. Delmas, The role of collagen in bone strength, Osteoporos. Int. 17 (3) (2006) 319–336.
[46] J. Bella, B. Brodsky, H.M. Berman, Hydration structure of a collagen peptide, Structure 3 (9) (Sep 15 1995) 893–906.
[47] I.A. Karampas, M.G. Orkoula, C.G. Kontoyannis, A quantitative bioapatite/collagen calibration method using Raman spectroscopy of bone, J. Biophotonics 6 (8) (Aug 2013) 573–586.
[48] M.R. Allen, E. Gineyts, D.J. Leeming, D.B. Burr, P.D. Delmas, Bisphosphonates alter trabecular bone collagen cross-linking and isomerization in beagle dog vertebra, Osteoporos. Int. 19 (3) (Mar 2008) 329–337.
[49] M. Saito, S. Mori, T. Mashiba, S. Komatsubara, K. Marumo, Collagen maturity, glycation induced-pentosidine, and mineralization are increased following 3-year treatment with incadronate in dogs, Osteoporos. Int. 19 (9) (Sep 2008) 1343–1354.
[50] E. Durchschlag, E.P. Paschalis, R. Zoehrer, P. Roschger, P. Fratzl, R. Recker, et al., Bone material properties in trabecular bone from human iliac crest biopsies after 3- and 5-year treatment with risedronate, J. Bone Miner. Res. 21 (10) (Oct 2006) 1581–1590.
[51] Y. Bala, B. Depalle, D. Farlay, T. Douillard, S. Meille, H. Follet, et al., Bone micromechanical properties are compromised during long-term alendronate therapy independently of mineralization, J. Bone Miner. Res. 27 (4) (Apr 2012) 825–834.
[52] S. Gamsjaeger, B. Buchinger, R. Zoehrer, R. Phipps, K. Klaushofer, E.P. Paschalis, Effects of one year daily teriparatide treatment on trabecular bone material properties in postmenopausal osteoporotic women previously treated with alendronate or risedronate, Bone 49 (6) (Dec 2011) 1160–1165.
[53] B. Hofstetter, S. Gamsjaeger, R.J. Phipps, R.R. Recker, F.H. Ebetino, K. Klaushofer, et al., Effects of alendronate and risedronate on bone material properties in actively forming trabecular bone surfaces, J. Bone Miner. Res. 27 (5) (May 2012) 995–1003.
[54] F.P. Coxon, K. Thompson, A.J. Roelofs, F.H. Ebetino, M.J. Rogers, Visualizing mineral binding and uptake of bisphosphonate by osteoclasts and non-resorbing cells, Bone 42 (5) (May 2008) 848–860.
[55] G.G. Reinholz, B. Getz, L. Pederson, E.S. Sanders, M. Subramaniam, J.N. Ingle, et al., Bisphosphonates directly regulate cell proliferation, differentiation, and gene expression in human osteoblasts, Cancer Res. 60 (21) (Nov 2000) 6001–6007.
[56] F. von Knoch, C. Jaquiery, M. Kowalsky, S. Schaeren, C. Alabre, I. Martin, et al., Effects of bisphosphonates on proliferation and osteoblast differentiation of human bone marrow stromal cells, Biomaterials 26 (34) (Dec 2005) 6941–6949.
[57] F.P. Koch, S.S. Yekta, C. Merkel, T. Ziebart, R. Smeets, The impact of bisphosphonates on the osteoblast proliferation and collagen gene expression in vitro, Head Face Med. 6 (2010) 12.
[58] F.G. Basso, A.P.S. Turrioni, J. Hebling, C.A. de Souza Costa, Effects of zoledronic acid on odontoblast-like cells, Arch. Oral Biol. 58 (5) (May 2013) 467–473.
[59] Y. Xiong, H.J. Yang, J. Feng, Z.L. Shi, L.D. Wu, Effects of alendronate on the proliferation and osteogenic differentiation of MG-63 cells, J. Int. Med. Res. 37 (2) (Apr 2009) 407–416.
[60] B. Frediani, A. Spreafico, C. Capperucci, F. Chellini, D. Gambera, P. Ferrata, et al., Long-term effects of neridronate on human osteoblastic cell cultures, Bone 35 (4) (Oct 2004) 859–869.
[61] B. Pan, To LB, A.N. Farrugia, D.M. Findlay, J. Green, S. Gronthos, et al., The nitrogen-containing bisphosphonate, zoledronic acid, increases mineralisation of human bone-derived cells in vitro, Bone 34 (1) (Jan 2004) 112–123.
[62] D.R. Eyre, M.A. Weis, Bone collagen: new clues to its mineralization mechanism from recessive osteogenesis imperfecta, Calcif. Tissue Int. 93 (4) (Oct 2013) 338–347.
[63] Y. Wang, T. Azaïs, M. Robin, A. Vallée, C. Catania, P. Legriel, et al., The predominant role of collagen in the nucleation, growth, structure and orientation of bone apatite, Nat. Mater. 11 (8) (Aug 2012) 724–733.
[64] N. Almora-Barrios, K.F. Austen, N.H. de Leeuw, Density functional theory study of the binding of glycine, proline, and hydroxyproline to the hydroxyapatite (0001) and (0110) surfaces, Langmuir ACS J. Surf. Colloids 25 (9) (May 5 2009) 5018–5025.
[65] A. Roschger, S. Gamsjaeger, B. Hofstetter, A. Masic, S. Blouin, P. Messmer, et al., Relationship between the v2PO4/amide III ratio assessed by Raman spectroscopy and the calcium content measured by quantitative backscattered electron microscopy in healthy human osteonal bone, J. Biomed. Opt. 19 (6) (Jun 11 2014) 65002.
[66] G.F. Muschler, V.P. Raut, T.E. Patterson, J.C. Wenke, J.O. Hollinger, The design and use of animal models for translational research in bone tissue engineering and regenerative medicine, Tissue Eng. B Rev. 16 (1) (Feb 2010) 123–145.
[67] J.T. Chang, L. Green, J. Beitz, Renal failure with the use of zoledronic acid, N. Engl. J. Med. 349 (17) (Oct 23 2003) (1676-1679-1679).
[68] G.S. Markowitz, P.L. Fine, J.I. Stack, C.L. Kunis, J. Radhakrishnan, W. Palecki, et al., Toxic acute tubular necrosis following treatment with zoledronate (Zometa), Kidney Int. 64 (1) (Jul 2003) 281–289.
[69] D. Henley, J. Kaye, J. Walsh, G. Cull, Symptomatic hypocalcaemia and renal impairment associated with bisphosphonate treatment in patients with multiple myeloma, Int. Med. J. 35 (12) (Dec 2005) 726–728.
[70] M. Bodmer, P. Amico, M.J. Mihatsch, M. Haschke, O. Kummer, S. Krähenbühl, et al., Focal segmental glomerulosclerosis associated with long-term treatment with zoledronate in a myeloma patient, Nephrol. Dial. Transplant. 22 (8) (Aug 2007) 2366–2370.
[71] T.K. Joensuu, Renal toxicity following zoledronic acid reversed with ibandronate in a prostate cancer patient with bone metastases, Urol. Int. 80 (4) (2008) 448–450.
[72] R. von Moos, Bisphosphonate treatment recommendations for oncologists, Oncologist 10 (Suppl. 1) (2005) 19–24.
[73] H.M. Weiss, U. Pfaar, A. Schweitzer, H. Wiegand, A. Skerjanec, H. Schran, Biodistribution and plasma protein binding of zoledronic acid, Drug. Metab. Dispos. Biol. Fate Chem. 36 (10) (2008 Oct) 2043–2049.